

State-of-Charge for Battery Management System via Kalman Filter

T. O. Ting, Ka Lok Man, Chi-Un Lei, Chao Lu

Abstract—Battery Management System (BMS) requires an indefinite accurate model. With an aging model, the lifetime of a battery can be precisely predicted with respect to the State-of-Charge (SoC) of a battery. The mathematical model in terms of state variables involving smart BMS is presented in this work. The state space model is crucial as an accurate model and is able to represent the complex dynamic behavior of a battery system. A numerical case study is done to verify the model obtained through mathematical derivations by adopting the prominent RC battery model from literature. Furthermore, the well-known Kalman filter (KF) is applied to estimate the SoC of a battery system. With accurate prediction of SoC of battery system, its lifetime could be prolonged, and thereby saving us substantial cost.

Index Terms—Battery Management System (BMS), battery modeling, Kalman filter, State-of-Charge, state space.

I. INTRODUCTION

THE understanding of a battery system is essential before efficient management system could be designed [1], [2], [3]. Hence, a generic tool to describe the battery performance under a wide variety of conditions and applications is highly desirable [1]. As such, the electrical modeling is able to provide such a tool that enables visualization of the processes occurring inside rechargeable batteries. Only with the presence of these generic models could new battery management system be developed for reliable performance. These algorithms control the operation and maintain the performance of battery packs. The ultimate aim is to prolong battery life and ensures reliable safety alongside many applications, especially in photovoltaic systems [4], [5], [6].

Battery modeling is done in many ways depending on the types of battery. In general, the resulted battery model is mathematical model comprising of numerous mathematical descriptions [7]. Ultimately, the battery models aim to determine State-of-Charge (SoC) of a battery system. However, the complexity of the nonlinear electrochemical processes has been a great barrier to modeling this dynamic process accurately. The accurate determination of SoC will enable the utilization of battery for optimal performance, long lifetime, and prevent irreversible physical damage to the battery [8]. Solutions to SoC via neural networks [9] and fuzzy logic [10] have been difficult and costly for online implementation due to large computation, causing the battery pack controller to

be heavily loaded. However, this can be a good alternative in the near future due to the increased computational power of processing chips alongside their declining cost.

Model-based state-estimation has been proposed in [11], [12], [13]. In [12] a state-estimation model had been utilized for the determination of optimized charging current using Genetic Algorithm (GA). In [14] Ant Colony algorithm was applied to determine the charging current in each stage to reduce charging time. In control theories, the well-known Kalman filter [15] had been applied successfully for both state observation and prediction problems [11]. Work in [16] utilized manufacturers' data in modeling the dynamic behavior of battery.

In this work, a mathematical derivation leading to a state space model is presented. The basic schematic model is adopted from [11], [13]. Hereby, a thorough analysis in the form of state variables with the application of Kalman filter is presented. The rest of the paper is organized as follows. Section II discusses the factors of battery aging. A mathematical model is derived in Section III, describing the state space model. Results are presented in Section V, and finally the conclusions are derived in Section VI.

II. BATTERY AGING

Identification of key aging parameters in battery models can validate degradation hypotheses and provide a foundation for estimation of battery status, e.g. State of Health (SOH). In brief, aging and degradation of batteries can be caused by capacity fading (the loss of battery charging/discharging capacity over time) as well as power fading (the loss of absorbing and delivering electrical power). From another perspective, power fading and energy fading are associated with impedance rise and capacity loss, respectively. Detailed discussion of typical aging effects can be found in [17]. A few major effects are outlined in the following subsections.

A. Thermal Degradation

The performance of a battery is significantly affected by temperature. For instance, Lithium battery can effectively operate between -30°C and 52°C . When the temperature drops below -30°C , diffusion and chemical reactions become inactive and thus battery impedance increases dramatically. On the other hand, when the temperature rises above 60°C , the battery has a significant capacity loss. Also, if the temperature rises above 85°C , the battery could be damaged easily. Chemical reactions in batteries grow exponentially when the temperature increases. Meanwhile, since vigorous chemical reactions generate excessive heat, the battery could also break down if the heat from batteries is not properly managed.

Manuscript received April 22, 2014; revised May 1, 2014. This work was supported by Xi'an Jiaotong-Liverpool University under RDF-13-01-13.

T. O. Ting is with the Department of Electrical and Electronic Engineering, Xian Jiaotong-Liverpool University, China. Email: toting@xjtlu.edu.cn

K. L. Man is with the Department of Computer Science and Software Engineering, Xian Jiaotong-Liverpool University, China and Department of Computer Science, Yonsei University, Korea. Email: ka.man@xjtlu.edu.cn

C.-U. Lei is with the Department of Electrical and Electronic Engineering, The University of Hong Kong, Hong Kong. Email: culei@eee.hku.hk

C. Lu is with Purdue University, West Lafayette, Indiana. Email: celuchao@gmail.com

B. Physical Damage

Battery aging can also be caused by electrode fracture and fatigue. In existing literatures, a specific electrode model and a diffusion-induced stress model have been proposed for investigation [18]. Results showed that the output voltage does not change significantly, however it increasingly accumulates stress.

C. Particles Accumulation

Solid Electrolyte Interphase (SEI) is formed on the surface of electrodes when the battery is charged, and in particular, when electrode starts to react with the electrolyte. SEI absorbs mobilized Lithium ions and slows down the transportation of ions between electrode and electrolyte. These form crystalline introduce power fading and capacity fading. In the case of low and high current densities, moss and dendrite are formed on the surface of negative electrode. These substances reduce surface area of electrodes for reactions, and thus causing battery fading.

D. Aging Characterization

Measurements are needed in order to accurately characterize aging in batteries. To investigate the cycle life capabilities of lithium ion battery cells during fast charging, cycle life tests have been carried out at different constant charge current rates. Through measurement results, cycle life models have been developed to predict the battery cycle ability. The analysis indicates that the cycle life of the battery degrades when the charge current rate increases. In addition, the measurement of battery impedance via electrochemical impedance spectroscopy (EIS) and the current-pulse technique [19] helps in determining battery health.

In order to ensure a uniform temperature during battery operations, maintaining battery performance, and eventually prolong the battery lifetime, real-time temperature sensing and monitoring systems as well as cooling systems are needed [20], [21], [22]. In addition, in order to improve cycle stability and battery capacity, thick anodes (e.g. about 1 mm) are adopted for Li-ion batteries. These anodes consist of vertically aligned carbon nanotubes which are coated with silicon and carbon [23].

E. Aging Models

Aging parameters in Lithium-ion batteries vary with different current rates, working temperatures and depths of discharge. For example, in order to model the thermal characteristics of the battery that causes battery aging, it is necessary to model the generation of heat inside the battery, heat transfer between battery and the environment, and the reactivity of chemical reactions with respect to the temperature [24]. In particular, in order to correctly model the thermal distribution and characteristics of battery packs, lumped thermal models are formulated to model the ohmic heating in battery cell packs [25]. The aging parameters can be applied for early aging detection. Through early detection and appropriate maintenance, performance of battery cells can be significantly improved. Detection can be done by analyzing real-time data from operations of batteries (e.g. voltage and current data from lithium-ion cells). In [12],

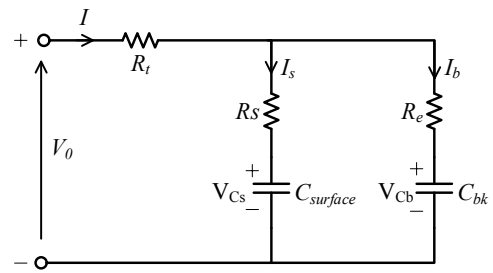


Fig. 1. Schematic of RC battery model

battery aging detection is done based on the sequential clustering of battery packs. During operations, a derived fuzzy model is used to predict operation performance and detect the aged battery via similarity comparisons, with respect to the ideal situation.

III. BATTERY MODEL [13]

Several battery models existed over the past years. Each of these models varies in term of its complexity and applications. In this work, a dynamical battery model is adopted, consisting of state variable equations, from [11], [13]. The schematic representation of this model is shown in Fig. 1. In this model, there exists a bulk capacitor C_{bk} that acts as a energy storage component in the form of charge, a capacitor that models the surface capacitance and diffusion effects within the cell $C_{surface}$, a terminal resistance R_t , surface resistance R_s , and end resistance R_e . The voltages across both capacitors are denoted as V_{Cb} and V_{Cs} , respectively.

A. Mathematical Derivations of Battery Model

In this derivation, we aim to form a state-space model consisting of the state variables V_{Cb} , V_{Cs} and V_0 . State variables are mathematical description of the "state" of a dynamic system. In practice, the state of a system is used to determine its future behaviour. Models that consist of paired first-order differential equations are in state-variable form.

Following the voltages and currents illustrated in Fig. 1, the terminal voltage V_0 can be expressed as

$$V_0 = IR_t + I_b R_e + V_{Cb}, \quad (1)$$

which is similar to

$$V_0 = IR_t + I_b R_s + V_{Cs}. \quad (2)$$

By equating the (1) and (2), and after simple algebraic manipulation, which results in

$$I_b R_e = I_s R_s + V_{Cs} - V_{Cb}. \quad (3)$$

From Kirchoff's laws, $I = I_b + I_s$,

$$I_s = I - I_b, \quad (4)$$

Substituting (4) into (3) yields

$$I_b (R_e + R_s) = IR_s + V_{Cs} - V_{Cb}. \quad (5)$$

By assuming a slow varying C_{bk} , that is $I_b = C_{bk} \dot{V}_{Cb}$ (from basic formula of $i = C \frac{\partial V}{\partial t}$) and substituting into (5), the following equation is obtained after rearrangement

$$\dot{V}_{Cb} = \frac{IR_s}{C_{bk}(R_e + R_s)} + \frac{V_{Cs}}{C_{bk}(R_e + R_s)} - \frac{V_{Cb}}{C_{bk}(R_e + R_s)}. \quad (6)$$

By applying a similar derivation, the rate of change of the surface capacitor voltage, derived also from (1) and (2) as

$$\dot{V}_{Cs} = \frac{IR_e}{C_{surface}(R_e + R_s)} - \frac{V_{Cs}}{C_{surface}(R_e + R_s)} + \frac{V_{Cb}}{C_{surface}(R_e + R_s)}. \quad (7)$$

By assuming $A = \frac{1}{C_{bk}(R_e + R_s)}$ and $B = \frac{1}{C_{surface}(R_e + R_s)}$, (6) and (7) can be written as

$$\dot{V}_{Cb} = A \cdot IR_s + A \cdot V_{Cs} - A \cdot V_{Cb}, \quad (8)$$

and

$$\dot{V}_{Cs} = B \cdot IR_e - B \cdot V_{Cs} + B \cdot V_{Cb}, \quad (9)$$

respectively. Further, (8) and (9) can be combined to form a state variable relating voltages V_{Cs} and V_{Cb} and current flow I , which is

$$\begin{bmatrix} \dot{V}_{Cb} \\ \dot{V}_{Cs} \end{bmatrix} = \begin{bmatrix} -A & A \\ B & -B \end{bmatrix} \begin{bmatrix} V_{Cb} \\ V_{Cs} \end{bmatrix} + \begin{bmatrix} A \cdot R_s \\ B \cdot R_e \end{bmatrix} I. \quad (10)$$

Next, the output voltage is derived from (1) and (2). By adding both equations, we obtain

$$2V_0 = 2IR_t + I_b R_e + I_s R_s + V_{Cb} + V_{Cs}. \quad (11)$$

By substituting $I_b = \frac{R_s}{R_s + R_e}$ and $I_s = \frac{R_e}{R_s + R_e}$ into (11), it is further simplified as

$$V_0 = \frac{V_{Cb} + V_{Cs}}{2} + \left(R_t + \frac{R_e R_s}{R_e + R_s} \right) I \quad (12)$$

By taking the time derivative of the output voltage and assuming $dI/dt \approx 0$ (this simply mean that the change rate of terminal current can be ignored when implemented digitally). Hence we get

$$\dot{V}_0 = \frac{\dot{V}_{Cb} + \dot{V}_{Cs}}{2}. \quad (13)$$

By substituting the values obtained earlier in (8) and (9) into (13), results in

$$2\dot{V}_0 = (-A + B)V_{Cb} + (A - B)V_{Cs} + (AR_s + BR_e)I. \quad (14)$$

Then, by solving for V_{Cs} from (12) we obtain

$$V_{Cs} = 2V_0 - 2\left(R_t + \frac{R_e R_s}{R_e + R_s}\right)I - V_{Cb}, \quad (15)$$

and after substitution into (14) yields

$$\dot{V}_0 = (-A + B)V_{Cb} + (A - B)V_0 + [A(0.5R_s + R_t + D) + B(0.5R_e - R_t - D)]I. \quad (16)$$

Finally, the complete state variable network is obtained by integrating (16) into (10), thus the complete state variable description of the network is obtained as

$$\begin{bmatrix} \dot{V}_{Cb} \\ \dot{V}_{Cs} \\ \dot{V}_0 \end{bmatrix} = \begin{bmatrix} -A & A & 0 \\ B & -B & 0 \\ (-A + B) & 0 & (A - B) \end{bmatrix} \begin{bmatrix} V_{Cb} \\ V_{Cs} \\ V_0 \end{bmatrix} + \begin{bmatrix} A \cdot R_s \\ B \cdot R_e \\ A(0.5R_s - R_t - D) + B(0.5R_e + R_t + D) \end{bmatrix} I, \quad (17)$$

whereby constants A , B and D have been given earlier and hereby restated as

$$\begin{bmatrix} A \\ B \\ D \end{bmatrix} = \begin{bmatrix} \frac{1}{C_{bk}(R_e + R_s)} \\ \frac{1}{C_{surface}(R_e + R_s)} \\ \frac{R_e R_s}{R_e + R_s} \end{bmatrix}. \quad (18)$$

This completes the initial derivation of a battery model.

B. Numerical Example

By substituting all capacitor and resistor values from Table I into (18), we obtain relevant values as

$$\begin{bmatrix} A \\ B \\ D \end{bmatrix} = \begin{bmatrix} 0.001508759347566 \\ 1.623837940973491 \\ 0.001875000000000 \end{bmatrix}. \quad (19)$$

By defining matrix M ,

$$M = \begin{bmatrix} -A & A & 0 \\ B & -B & 0 \\ (-A + B) & 0 & (A - B) \end{bmatrix}, \quad (20)$$

and

$$N = \begin{bmatrix} A \cdot R_s \\ B \cdot R_e \\ A(0.5R_s - R_t - D) + B(0.5R_e + R_t + D) \end{bmatrix}, \quad (21)$$

again by substituting all the values from Table I and calculated A , B and D , we obtain the value of M as

$$M = \begin{bmatrix} -1.51 \times 10^{-3} & 1.51 \times 10^{-3} & 0 \\ 1.6238 & -1.6238 & 0 \\ 1.6223 & 0 & -1.6223 \end{bmatrix}, \quad (22)$$

and N as

$$N = \begin{bmatrix} 5.66 \times 10^{-6} \\ 6.08 \times 10^{-3} \\ 1.05 \times 10^{-2} \end{bmatrix}. \quad (23)$$

As such (17) can be rewritten as

$$\begin{bmatrix} \dot{V}_{Cb} \\ \dot{V}_{Cs} \\ \dot{V}_0 \end{bmatrix} = M \cdot \begin{bmatrix} V_{Cb} \\ V_{Cs} \\ V_0 \end{bmatrix} + N \cdot I, \quad (24)$$

or numerically as

$$\begin{bmatrix} \dot{V}_{Cb} \\ \dot{V}_{Cs} \\ \dot{V}_0 \end{bmatrix} = \begin{bmatrix} -0.0015 & 0.0015 & 0 \\ 1.6238 & -1.6238 & 0 \\ 1.6223 & 0 & -1.6223 \end{bmatrix} \cdot \begin{bmatrix} V_{Cb} \\ V_{Cs} \\ V_0 \end{bmatrix} + \begin{bmatrix} 5.66 \times 10^{-6} \\ 6.08 \times 10^{-3} \\ 1.05 \times 10^{-2} \end{bmatrix} \cdot I \quad (25)$$

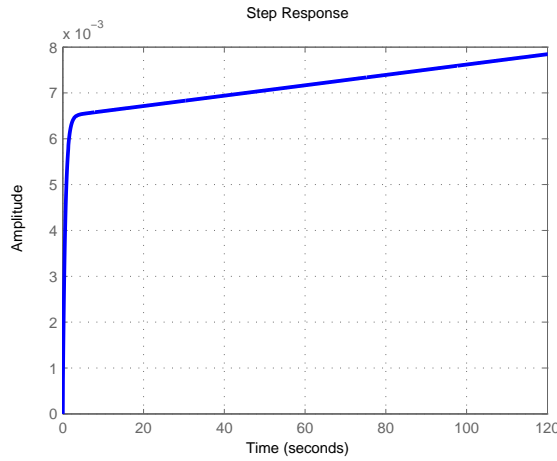


Fig. 2. Output response of RC model due to constant input.

C. State Space Modeling

Based on control theories, a lumped linear network can be written in the form

$$\begin{aligned} \dot{x}(t) &= \mathbf{A}x(t) + \mathbf{B}u(t), \\ y(t) &= \mathbf{C}x(t) + \mathbf{D}u(t). \end{aligned} \quad (26)$$

where in this work, the state variable $\dot{x}(t)$ is

$$\dot{x}(t) = \begin{bmatrix} \dot{V}_{Cb} \\ \dot{V}_{Cs} \\ \dot{V}_0 \end{bmatrix}. \quad (27)$$

Obviously,

$$x(t) = \begin{bmatrix} V_{Cb} \\ V_{Cs} \\ V_0 \end{bmatrix}, \quad (28)$$

with

$$u(t) = I, \quad (29)$$

and the output $y(t)$ is given as

$$y(t) = V_0. \quad (30)$$

This means that the output of the system is the open terminal voltage that we wanted, as expected. Also, by comparing (37) and (24), it is easily noted that $\mathbf{A} = \mathbf{M}$, that is

$$\mathbf{A} = \begin{bmatrix} -1.51 \times 10^{-3} & 1.51 \times 10^{-3} & 0 \\ 1.6238 & -1.6238 & 0 \\ 1.6223 & 0 & -1.6223 \end{bmatrix}, \quad (31)$$

and $\mathbf{B} = \mathbf{N}$, which is

$$\mathbf{B} = \begin{bmatrix} 5.66 \times 10^{-6} \\ 6.08 \times 10^{-3} \\ 1.05 \times 10^{-2} \end{bmatrix}, \quad (32)$$

while

$$\mathbf{C} = [0 \ 0 \ 1], \quad (33)$$

and the last one,

$$\mathbf{D} = [0]. \quad (34)$$

Further, the above state space variables are transformed to a transfer function, $G(s)$. This is done by using `ss2tf` function in Matlab, and thereby, after factorization yielding

$$G(s) = \frac{0.01054s^2 + 0.0171s + 2.981 \times 10^{-5}}{s^3 + 3.248s^2 + 2.637s - 1.144 \times 10^{-18}} \quad (35)$$

The plot of the unit step response for the gain in (35) is given in Fig. 2. Basically, it shows that the open circuit terminal voltage V_0 in Fig. 1 increases linearly during charging operation in a very slow manner after transient behaviour for a few seconds.

TABLE I
PARAMETERS FOR CELL MODEL [11], [13]

C_{bk}	$C_{surface}$	R_e	R_s	R_t
88372.83 F	82.11 F	0.00375 Ω	0.00375 Ω	0.002745 Ω

D. Observability of the RC Battery Model

In control theory, observability is a degree in predicting the internal states of a system via its external outputs. As such, for an observable system, the behaviour of the entire system can be predicted via the system's outputs. On the other hand, if a system is not observable, the current values of some of its states cannot be estimated through output signal. This means that the controller does not know the states' values. In theory, the observability of a system can be determined by constructing observability matrix O_b .

$$O_b = \begin{bmatrix} \mathbf{C} \\ \mathbf{C}\mathbf{A} \\ \mathbf{C}\mathbf{A}^2 \\ \vdots \\ \mathbf{C}\mathbf{A}^{n-1} \end{bmatrix},$$

and a system is said to be observable if the row rank of O_b is equal to n (this is also known as full rank matrix). The ultimate rationale of such test is that if n rows are linearly independent, then each of the n states is viewable through linear combinations of the output $y(t)$.

Further, by substituting all \mathbf{A} , \mathbf{B} , \mathbf{C} and \mathbf{D} values from (31)-(34), we obtain

$$O_b = \begin{bmatrix} 0 & 0 & 1 \\ 1.6223 & 0 & -1.6223 \\ -2.6344 & 0.0024 & 2.6320 \end{bmatrix}. \quad (36)$$

Clearly, in this case O_b is a full rank matrix, which concludes that this system is observable.

IV. KALMAN FILTER FOR SOC ESTIMATION

As given in (??), a continuous time-invariant linear system can be described in state variable form as

$$\begin{aligned} \dot{x}(t) &= \mathbf{A}x(t) + \mathbf{B}u(t), \\ y(t) &= \mathbf{C}x(t). \end{aligned} \quad (37)$$

where

- u input vector,
- x is the state vector,
- y is the output vector,
- \mathbf{A} is the time invariant dynamic matrix,
- \mathbf{B} is the time invariant input matrix,
- \mathbf{C} is the time invariant measurement matrix.

If we assume that the applied input u is constant during each sampling interval, a discrete-time equivalent model of the system will now be

$$\begin{aligned} x(n+1) &= \mathbf{A}_d \cdot x(n) + \mathbf{B}_d \cdot u(n) \\ y(n+1) &= \mathbf{C}_d \cdot x(n+1) \end{aligned} \quad (38)$$

where

$$\mathbf{A}_d \approx \mathbf{I} + \mathbf{A} \cdot T_c, \quad \mathbf{B}_d = \mathbf{B} \cdot T_c, \quad \mathbf{C}_d = \mathbf{C}, \quad (39)$$

where \mathbf{I} is the identity matrix and T_c is the sampling period. As for this system, two noises are present which are additive Gaussian noise,

- \mathbf{w} vector representing system disturbances and model inaccuracies, and
- \mathbf{v} vector representing the effects of measurement noise.

Both \mathbf{w} and \mathbf{v} have a mean value of zero and the following covariance matrices

$$\begin{aligned} E[\mathbf{w} \cdot \mathbf{w}^T] &= \mathbf{Q}, \\ E[\mathbf{v} \cdot \mathbf{v}^T] &= \mathbf{R}, \end{aligned} \quad (40)$$

where E denotes the expectation (or mean) operator and superscript T means the transpose of the respective vectors. In usual case, \mathbf{Q} and \mathbf{R} are normally set to a constant before simulation; in our case both are set to one (see Section V). By inclusion of these noises, the resulting system is now can be described by

$$\begin{aligned} x(n+1) &= \mathbf{A}_d \cdot x(n) + \mathbf{B}_d \cdot u(n) + \mathbf{w} \\ y(n+1) &= \mathbf{C}_d \cdot x(n+1) + \mathbf{v}, \end{aligned} \quad (41)$$

which is illustrated in Fig. (3)

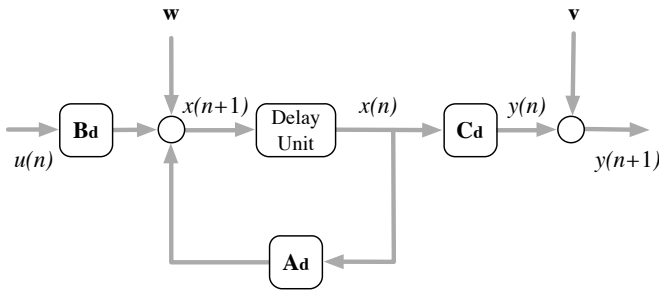


Fig. 3. Discrete system model with noises \mathbf{w} and \mathbf{v}

A. Property of Kalman filter

An important property of Kalman filter (KF) is that it minimizes the sum-of-squared errors between the actual value x and estimated states \hat{x} , given as

$$f_{min}(x) = E([x - \hat{x}] \cdot [x - \hat{x}]^T) \quad (42)$$

To understand the operations of KF, the meaning of the notation $\hat{x}(m|n)$ is crucial. It simply means that the estimate of x at event m takes into account all the discrete events up to event n . As such, (43) can include such information, now expanded as

$$f_{min}(x) = E([x(n) - \hat{x}(n|n)] \cdot [x(n) - \hat{x}(n|n)]^T) \quad (43)$$

In recursive implementation of KF, the current estimate $\hat{x}(n|n)$, together with the input $u(n)$ and measurement signals $y(n)$ are used for further estimating $\hat{x}(n+1|n+1)$.

B. KF Online Implementation

In the case of battery, it is well understood that only the terminal quantities can be measured (terminal voltage V_0 and current I). Assuming that battery parameters are time-invariant quantities, the recursive KF algorithm is applied. By applying (39) into (31)-(33), we obtain the following updated matrices, with $T_c = 1$:

$$\begin{aligned} \mathbf{A}_d &= \begin{bmatrix} 0.9984 & 1.51 \times 10^{-3} & 0 \\ 1.6238 & 0.6238 & 0 \\ 1.6223 & 0 & 0.6223 \end{bmatrix}, \\ \mathbf{B}_d &= \begin{bmatrix} 5.66 \times 10^{-6} \\ 6.08 \times 10^{-3} \\ 1.05 \times 10^{-2} \end{bmatrix}, \\ \mathbf{C}_d &= [0 \ 0 \ 1]. \end{aligned} \quad (44)$$

Note that \mathbf{B}_d and \mathbf{C}_d remain similar to its previous values, as given in (32) and (33).

V. RESULTS

The program, implemented in Matlab language is given in Appendix A to clarify the results obtained in this work. The output of the program is given as Appendix B, hereby shortened to save printing page. Some important results obtained in this work are available in this part. Note that \mathbf{Q} and \mathbf{R} mentioned in (40) are both set to one. The results obtained are tabulated in Table II. From these results, the Root-Mean-Squared (RMS) of the estimated error, which is the error from Kalman filter is far smaller compared to the measured error, with values of 1.0013 V and 1.92×10^{-4} V respectively. The time plot of this error from 0s to 60000s is shown in Fig. 4, depicting very small amplitude (≈ 0.04 V) along the timeline.

TABLE II
RECORDED RMS ERROR

RMS Error	Value
Measurement, $y - y_v$	1.00136010496
Estimated (KF), $y - y_e$	1.91859×10^{-4}

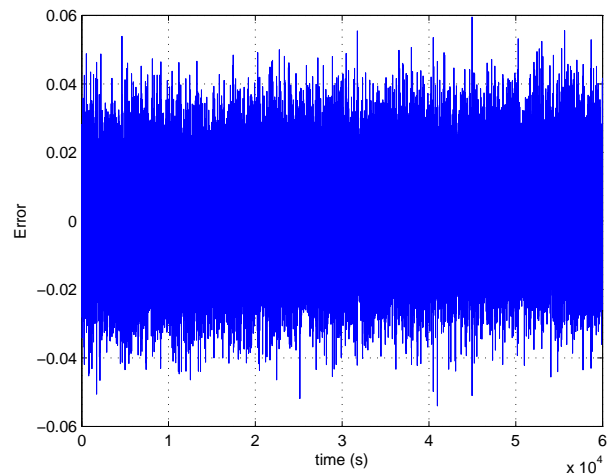


Fig. 4. The voltage error recorded, $Err = v(t) - \hat{v}(t)$.

A. Charging Behaviour

The charging characteristic is illustrated in Fig. 5 whereby the initial terminal voltage V_0 starts from 0 V up to approximately 1 V (1.045 V to be exact) within 60000 seconds (which is 100 minutes). This, as expected, is a time consuming process as in usual case it may take hours for an aqueous battery (lead acid) to be completely charged.

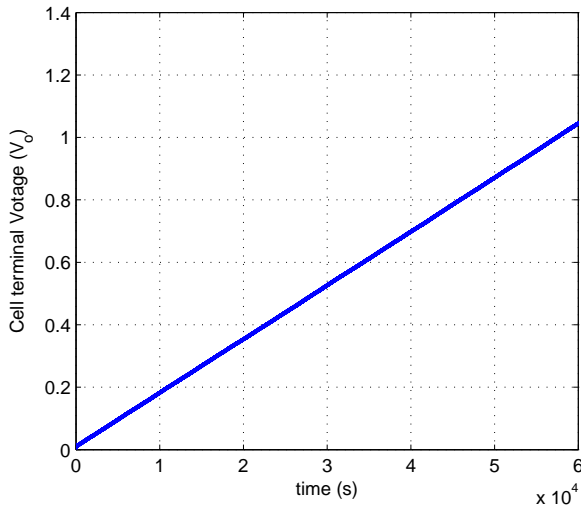


Fig. 5. Dynamic behavior of KF estimator with charge constant current of 1.53 A.

B. Discharging

For discharging process, the initial value of terminal voltage, $y_0 = V_0$ is set to 2.2 V in the Matlab program. The dynamic behaviour showing the discharge characteristic is shown in Fig. 6. From this figure, it is observed that the discharge process is similar to charging; but now with linearly decreasing V_0 slope. The open terminal voltage V_0 drops from 2.2 V to 1.2 V in 60000 seconds (100 minutes); this is similar to the charging process as it literally takes 100 minutes to reach $V_0 = 1$ V from zero potential.

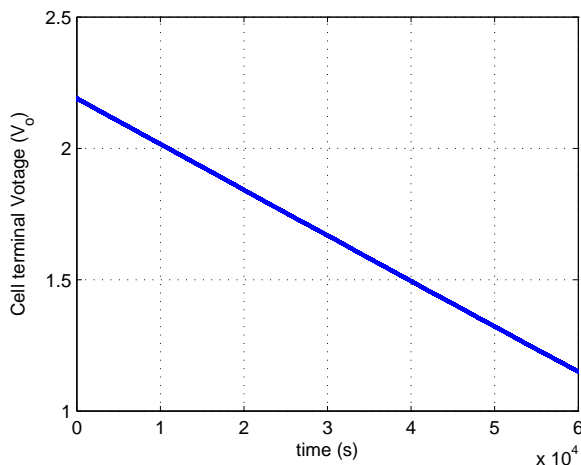


Fig. 6. Dynamic behavior of KF estimator with discharge constant current of -1.53 A.

VI. CONCLUSION

In this work, the factors of battery aging are discussed in details. Subsequently, we successfully obtain the state variables of the RC model that represents a battery in terms of mathematical derivations. The derivations come to a conclusion that there exists four state variables relevant to battery model. Further, based on control theories, we successfully plotted the response of the system, depicting a linearly increasing characteristic. With this state-estimation model, a prominent technique known as Kalman filter is applied with the aim of estimating State-of-Charge of Battery Management System. From numerical results, KF is more accurate in predicting the dynamic. This is shown by very small RMS error of the estimated error in comparison to its measurement error.

ACKNOWLEDGMENT

We appreciate the generosity of our colleagues, Nan Zhang and Sanghyuk Lee in sharing their expertise knowledge, contributing to the success of this work.

APPENDIX

A. Matlab source code

```
format long;
%Value for resistors and capacitors
Csurface=82.11;
Cbk=88372.83;
Re=0.00375;
Rs=0.00375;
Rt=0.002745;

a=1/(Cbk*(Re+Rs));
b=1/(Csurface*(Re+Rs));
d=(Re*Rs)/(Re+Rs);

%State variable matrices
A=[-a a 0 ; b -b 0 ; (-a+b) 0 (a-b) ]
B=[a*Re; b*Re;
    a*(0.5*Rs-Rt-d)+ b*(0.5*Re+Rt+d)]
C=[0 0 1 ]
D=[0]

%Transfer function
figure(1); %Figure 1
[num, den]=ss2tf(A,B,C,D,1)
G=tf(num,den)
step(G),grid;

% For Kalman filter:
% Identity matrix + diagonal element
A=[1-a a 0 ; b 1-b 0 ; (-a+b) 0 1+(a-b) ]
B=[a*Re; b*Re;
    a*(0.5*Rs-Rt-d)+ b*(0.5*Re+Rt+d)]
C=[0 0 1 ]

Tc=1;
A=A*Tc;
B=B*Tc;
C=C;
```

```

% Sample time=-1 for discrete model
Plant = ss(A,[B B],C,0,-1,...
    'inputname',{'u' 'w'},...
    'outputname','y');

Q = 1; R = 1;
[kalmf,L,P,M] = kalman(Plant,Q,R);
kalmf = kalmf(1,:);
kalmf

a = A;
b = [B B 0*B];
c = [C;C];
d = [0 0 0;0 0 1];
P = ss(a,b,c,d,-1,...
    'inputname',{'u' 'w' 'v'},...
    'outputname',{'y' 'yv'});

% Parallel connection of outputs ye and y
sys = parallel(P,kalmf,1,1,[],[])

% Close loop around input #4 and output #2
SimModel = feedback(sys,1,4,2,1)

% Delete yv from I/O list
SimModel = SimModel([1 3],[1 2 3])
SimModel.inputname

t = [0:60000]';
u(:) = -1.53; % Current for discharge

n = length(t)
randn('seed',0)
w = sqrt(Q)*randn(n,1);
v = sqrt(R)*randn(n,1);

[out,x] = lsim(SimModel,[w,v,u]);
y0=2.2; %This is initial terminal voltage
y = out(:,1)+y0; % true response,
ye = out(:,2)+y0; % filtered response
yv = y + v; % measured response

figure(2); %Figure 2
%plot(t,y,'g--',t,ye,'b-'), grid on;
plot(t,ye,'b-'), grid on;
xlabel('time (s)'),
ylabel('Cell terminal Votage (V_o)')

%Kalman filter response
figure(3); %Figure 3
plot(t,y-ye,'b-'), grid on;
xlabel('time (s)'), ylabel('Error')

%Calculate Errors
MeasErr = y-yv; %Measurement error
MeasErrCov= ...
sum(MeasErr.*MeasErr)/length(MeasErr);
EstErr = y-ye; %Estimated error
EstErrCov = ...
sum(EstErr.*EstErr)/length(EstErr);

```

```

%Display onto screen
MeasErrCov %Measurement error
EstErrCov %Estimated error

```

B. Simulation Output (shorten to save printed space)

The output of the run is show below, hereby only the essential components are shown.

```

Transfer function:
0.01054 s^2 + 0.01714 s + 2.981e-005
-----
s^3 + 3.248 s^2 + 2.637 s - 1.144e-018

A =
0.99849124    0.00150875    0
1.62383794   -0.62383794    0
1.62232918    0   -0.62232918

B =
0.000005657847553
0.006089392278651
0.010542685882214

C =
0    0    1
.
.
.

MeasErrCov =1.001360104960092
EstErrCov = 1.918588914886020e-004

```

REFERENCES

- [1] P. H. L. Notten and D. Danilov, "From battery modeling to battery management," in *2011 IEEE 33rd International Telecommunications Energy Conference (INTELEC)*, 2011, pp. 1–8.
- [2] C. Chen, K. L. Man, T. O. Ting, C. U. Lei, T. Krilavicius, T. T. Jeong, J. K. Seon, S. U. Guan, and P. W. H. Wong, "Design and realization of a smart battery management system," in *Proc of Intl MultiConference of Engineers and Computer Scientists*, vol. 2, 2012, pp. 1173–1176.
- [3] K. L. Man, K. Wan, T. O. Ting, C. Chen, T. Krilavicius, J. Chang, and S. H. Poon, "Towards a hybrid approach to soc estimation for a smart battery management system (BMS) and battery supported cyber-physical systems (CPS)," in *2nd Baltic Congress on Future Internet Communications (BCFIC)*, 2012, pp. 113–116.
- [4] D. Benchetrite, F. Mattera, M. Perrin, J. L. Martin, O. Bach, M. Le Gall, and P. Malbranche, "Optimization of charge parameters for lead acid batteries used in photovoltaic systems," in *Proceedings of 3rd World Conference on Photovoltaic Energy Conversion*, vol. 3, 2003, pp. 2408–2410 Vol.3.
- [5] T. O. Ting, K. L. Man, S.-U. Guan, T. T. Jeong, J. K. Seon, and P. W. H. Wong, "Maximum power point tracking (MPPT) via weightless swarm algorithm (WSA) on cloudy days," in *2012 IEEE Asia Pacific Conference on Circuits and Systems (APCCAS)*, 2012, pp. 336–339.
- [6] J. Ma, T. O. Ting, K. L. Man, N. Zhang, S. U. Guan, and P. W. H. Wong, "Parameter estimation of photovoltaic models via cuckoo search," *J. Appl. Math.*, vol. 2013, 2013.
- [7] H. Gu, "Mathematical modeling in lead-acid battery development," in *Proceedings of the Sixth Annual Battery Conference on Applications and Advances*, 1991, pp. 47–56.
- [8] C. S. Moo, K. S. Ng, Y. P. Chen, and Y. C. Hsieh, "State-of-Charge estimation with Open-Circuit-Voltage for lead-acid batteries," in *Power Conversion Conference - Nagoya. PCC '07*, 2007, pp. 758–762.
- [9] C. C. Chan, E. W. C. Lo, and S. Weixiang, "Available capacity computation model based on artificial neural network for lead-acid batteries in electric vehicles," *J. Power Sources*, vol. 87, no. 1, pp. 201–204, 2000.

- [10] P. Singh, C. F. Jr, and D. Reisner, "Fuzzy logic modelling of state-of-charge and available capacity of nickel/metal hydride batteries," *J. Power Sources*, vol. 136, no. 2, pp. 322–333, 2004.
- [11] B. S. Bhangu, P. Bentley, D. A. Stone, and C. M. Bingham, "Nonlinear observers for predicting state-of-charge and state-of-health of lead-acid batteries for hybrid-electric vehicles," *IEEE Trans. Veh. Technol.*, vol. 54, no. 3, pp. 783–794, 2005.
- [12] H. Saberi and F. R. Salmasi, "Genetic optimization of charging current for lead-acid batteries in hybrid electric vehicles," in *International Conference on Electrical Machines and Systems, ICEMS, 2007*, pp. 2028–2032.
- [13] T. O. Ting, K. L. Man, N. Zhang, C.-U. Lei, and C. Lu, "State-space battery modeling for smart battery management system," in *Lecture Notes in Engineering and Computer Science: Proceedings of The International MultiConference of Engineers and Computer Scientists 2014*, pp. 866–869.
- [14] Y.-H. Liu, J.-H. Teng, and Y.-C. Lin, "Search for an optimal rapid charging pattern for lithium-ion batteries using ant colony system algorithm," *IEEE Trans. Ind. Electron.*, vol. 52, no. 5, pp. 1328–1336, 2005.
- [15] R. E. Kalman *et al.*, "A new approach to linear filtering and prediction problems," *Journal of Basic Engineering*, vol. 82, no. 1, pp. 35–45, 1960.
- [16] N. K. Medora and A. Kusko, "Dynamic battery modeling of lead-acid batteries using manufacturers' data," in *27th International Telecommunications Conference. INTELEC '05, 2005*, pp. 227–232.
- [17] J. Vetter, P. Novák, M. R. Wagner, C. Veit, K. C. Möller, J. O. Besenhard, M. Winter, M. Wohlfahrt-Mehrens, C. Vogler, and A. Hammouche, "Ageing mechanisms in lithium-ion batteries," *J. Power Sources*, vol. 147, no. 1–2, pp. 269–281, 2005.
- [18] J. Christensen, "Modeling diffusion-induced stress in li-ion cells with porous electrodes," *J. Electrochem. Soc.*, vol. 157, no. 3, pp. A366–A380, 2010.
- [19] W. Waag, S. Käbitz, and D. U. Sauer, "Experimental investigation of the lithium-ion battery impedance characteristic at various conditions and aging states and its influence on the application," *Appl. Energy*, vol. 102, pp. 885–897, 2013.
- [20] R. Kizilel, R. Sabbah, J. R. Selman, and S. Al-Hallaj, "An alternative cooling system to enhance the safety of li-ion battery packs," *J. Power Sources*, vol. 194, no. 2, pp. 1105–1112, 2009.
- [21] R. Mahamud and C. Park, "Reciprocating air flow for li-ion battery thermal management to improve temperature uniformity," *J. Power Sources*, vol. 196, no. 13, pp. 5685–5696, 2011.
- [22] S. Al-Hallaj and J. R. Selman, "Thermal modeling of secondary lithium batteries for electric vehicle/hybrid electric vehicle applications," *J. Power Sources*, vol. 110, no. 2, pp. 341–348, 2002.
- [23] K. Evanoff, J. Khan, A. A. Balandin, A. Magasinski, W. J. Ready, T. F. Fuller, and G. Yushin, "Towards ultrathick battery electrodes: Aligned carbon nanotube-enabled architecture," *Adv. Mater.*, vol. 24, no. 4, pp. 533–537, 2012.
- [24] M. Doyle, T. Fuller, and J. Newman, "Modeling of galvanostatic charge and discharge of the lithium/ polymer/insertion cell," *J. Electrochem. Soc.*, vol. 140, no. 6, pp. 1526–1533, 1993.
- [25] K. Smith and C.-Y. Wang, "Power and thermal characterization of a lithium-ion battery pack for hybrid-electric vehicles," *J. Power Sources*, vol. 160, no. 1, pp. 662–673, 2006.